Viscoelastic Effects in Multilayer Polymer Extrusion

Patrick D. Anderson[1*], Joseph Dooley[2], Han E.H. Meijer[1]

[1] Materials Technology, Eindhoven University of Technology, P.O. Box 513, WH 4.142,
5600 MB Eindhoven, The Netherlands
[2] The Dow Chemical Company, 433 Building, Midland, Michigan, USA

* e-mail: p.d.anderson@tue.nl
Fax: x31.40.2447355

Received: 25.2.2006, Final version: 31.5.2006

Abstract:
The effect of viscoelasticity on multilayer polymer extrusion is discussed. In these coextrusion processes predetermined patterns are created with a remarkable breadth of complexity even in geometrically simple dies via elastic rearrangements caused by the second-normal stress differences. A computational method is offered, based on the mapping method, which quantitatively describes the flow-induced patterns. Besides that the results are esthetically beautiful, they are also relevant for practice, since process and die design optimization is now possible. Not only to minimize interface distortion, but potentially also to deliberately create new processes and products based on this flow-induced patterning of polymers.

Zusammenfassung:
Der Einfluss der Viskoelastizität auf die Mehrschichtextrusion bei Polymeren wird diskutiert. Bei diesen Koextrusionsprozessen werden vorher bestimmte Muster mit einer bemerkenswerten Komplexitätsvielfalt erzeugt, sogar in geometrisch einfachen Düsen mit Hilfe elastischer Umlagerungen, die durch die zweite Normalspannungsdifferenz erzeugt werden. Eine numerische Methode, die auf der Abbildungsmethode basiert, wird dargestellt, die die strömungsinduzierten Muster quantitativ beschreibt. Die Resultate sind nicht nur ästhetisch schön, sondern auch für die Praxis relevant, da die Optimierung des Prozess- und Düsendesigns nun möglich ist – nicht nur um die Verzerrung der Grenzfläche zu minimieren, sondern um möglicherweise auch gezielt neue Prozesse und Produkte zu schaffen, die auf der strömungsinduzierten Musterbildung bei Polymeren basieren.

Résumé:
L'effet de la viscoélasticité sur l'extrusion de polymères multicouches est discuté. Dans ces procédés de co-extrusion, des empreintes prédéterminées sont créées qui possèdent une gamme remarquablement étendue de complexité et ceci même pour des filières à géométrie simple. Ces empreintes sont associées à des réarrangements élastiques causés par la seconde différence de contraintes normales. Une méthode de calcul numérique est proposée, basée sur la méthode de cartographie qui décrit quantitativement les empreintes induites par l'écoulement. En plus de l'obtention de résultats esthétiquement magnifiques, ceux-ci sont pertinents pour ce qui concerne la pratique, puisque l'optimisation des procédés ainsi que des conceptions des filières est maintenant possible. Non seulement est-il possible de minimiser les distorsions d'interface, mais aussi de nouveaux procédés et produits peuvent être potentiellement créés de manière délibérée grâce à cette technique d'empreintes de polymères induites par l'écoulement.

Key words: extrusion, rheology, secondary flow, normal stresses, pattern formation

1 INTRODUCTION

Multilayer coextrusion is a process in which polymers are extruded and joined together in a feedblock or a die with the purpose of forming a single structure with multiple layers. The attraction of coextrusion is both economic and technical as it is a single-step process. Starting with two or more polymer materials, that are simultaneously extruded and shaped in a single die, a multilayer sheet or film can be formed. Coextrusion avoids the costs and complexities of conventional multistep lamination and coating processes, where individual plies must be made separately, and then primed, coated, and laminated. Moreover, coextrusion readily makes it possible to manufacture products with layers thinner than can be made and handled as an individual ply. Consequently, only the necessary thickness of a high performance polymer is used to meet a particular specification of the product. In fact, coextrusion has been used commercially to manufacture unique films consisting of hundreds of layers with individual layer thicknesses less than 100 nm. In an academic setup in our Eindhoven laboratory even individual layer thicknesses less than 40 nm have been reached using a multiflux static mixer. It is difficult to imagine another practical method of manufacturing these nanolayered structures.

Layers may be used to place colors, bury recycle, screen ultraviolet radiation, or to provide barrier properties, minimize die-face buildup, and to control film-surface properties, for example. Additives, such as antiblock, antislip, and antistatic agents, can be placed at specific layer positions. High melt strength layers can carry low melt strength materials during fabrication. Unfortunately, the best designed die or feedblock does not necessarily ensure a commercially acceptable product. Layered melt streams flowing through a coextrusion die can spread nonuniformly or can become unstable leading to layer nonuniformities and even intermixing of layers under certain conditions. The causes of these instabilities are related to non-Newtonian flow properties of polymers and viscoelastic interactions.

Coextruded layers normally should have uniform thicknesses throughout the structure for optimal performance. However, layer thickness non-uniformities have been observed in many commercial coextruded structures. Previous work has shown that layer thickness variations can occur for many reasons.

Several of the primary causes of layer thickness variations are interlayer instabilities, viscous encapsulation, and elastic layer rearrangement. Interfacial instability is an unsteady-state process in which the interface location between layers varies locally in a transient manner. Viscous encapsulation is a phenomenon in which a less viscous polymer will tend to encapsulate a more viscous polymer as they flow through a channel. Elastic layer rearrangement occurs when elastic polymers flow through non-radially symmetric geometries producing secondary flows which drive rearrangement of the layer thicknesses. These layer thickness variations have been studied experimentally [1 - 4] and numerically [5 - 9].

Interfacial instability in a number of coextruded polymer systems has been experimentally correlated with viscosity ratios and elasticity ratios [10], and a simplified rheology review has been given [11]. Other studies have looked at viscosity differences [12 - 14], surface tension [15], critical stress levels [16 - 18], viscosity model parameters [19 - 21], and elasticity [22, 23]. The work of Dooley clearly separates the effects interlayer instabilities, viscous encapsulation, and elastic layer rearrangement on layer thickness variations via a systematic approach [24].

In this paper we examine the layer uniformity of coextruded structures with similar viscosities. The finite element method is used to simulate the flow of viscoelastic polymers in different channel geometries and the location of the coextruded interface is determined using the mapping method. Finally, a quantification of the influence of second-normal stress differences on the resulting secondary flow is given.

2 MATHEMATICAL EQUATIONS AND NUMERICAL METHOD

The momentum and continuity equation for the steady state flow of an incompressible viscoelastic fluid are given by

$$-\nabla p + \nabla \cdot \boldsymbol{\tau} = 0 \tag{1}$$

$$\nabla \cdot \boldsymbol{u} = 0 \tag{2}$$

where p is the pressure field, $\boldsymbol{\tau}$ is the viscoelastic extra-stress tensor, and $\boldsymbol{u}$ is the velocity field. Inertial and volume forces are assumed to be negligible.

If a discrete spectrum of N relaxation times is used then $\boldsymbol{\tau}$ can be decomposed as follows:

$$\boldsymbol{\tau} = \sum_{i=1}^{N} \boldsymbol{\tau}_i$$

where $\boldsymbol{\tau}_i$ is the contribution of the i^{th} relaxation time to the viscoelastic stress tensor. For the extra stress contributions $\boldsymbol{\tau}_i$, a constitutive equation must be chosen.

A realistic viscoelastic equation that at least describes second-normal stress differences in flow is the Giesekus constitutive equation that takes the form

$$\boldsymbol{\tau}_i \left[\boldsymbol{I} + \frac{\alpha_i \lambda_i}{\eta_i} \boldsymbol{\tau}_i \right] + \lambda_i \overset{\nabla}{\boldsymbol{\tau}}_i = 2\eta_i \boldsymbol{D} \tag{3}$$

where λ_i is the relaxation time, η_i is the viscosity factor of the i^{th} mode. $\boldsymbol{D}$ is rate of deformation tensor,

$$\boldsymbol{D} = \frac{1}{2}\left(\nabla \boldsymbol{u} + \nabla \boldsymbol{u}^T\right)$$

and the upper triangle stands for the upper-convected time derivative operator defined as,

$$\overset{\nabla}{\boldsymbol{\tau}} \equiv \frac{\partial \boldsymbol{\tau}}{\partial t} + u \cdot \nabla \boldsymbol{\tau} - \left(\nabla \boldsymbol{u}\right)^T \cdot \tau - \tau \cdot \nabla \boldsymbol{u} \tag{4}$$

The symbol $\boldsymbol{I}$ denotes the unit tensor. In Eq. 3, α_i are additional material parameters of the model, which control the ratio of the second to the first-normal stress difference. In particular, for low shear rates, $\alpha_1 = -2N_2/N_1$, where α_1 is associated with the highest relaxation time λ_i and N_1, N_2 represent the first and second-normal stress difference, respectively. The set of partial differential Eqs. 1 - 3 are completed with initial and boundary conditions.

In the community of viscoelastic flow computations great effort has been made to develop numerical methods to accurately solve the full set of equations for increasing levels of elasticity. In the absence of a solvent viscosity the momentum equation looses its ellipticity which has direct consequences for any finite element method. The constitutive equation is a hyperbolic partial differential equation which requires special attention. Two suitable techniques to deal with the constitutive equations are discontinuous Galerkin (DG) and streamline upwinding (SUPG). In this work the latter method is used.

One of the standard approaches to retain ellipticity of the momentum equation is the DEVSS formulation, see Problem 1 below. A great advantage of this method over other techniques (like EVSS) is that the objective derivative of the rate of strain tensor is avoided and the method is not restricted to a particular class of constitutive equations. In the discrete momentum Eq. 6, an elliptic operator $2\bar{\eta}(\boldsymbol{D} - \bar{\boldsymbol{D}})$ is introduced, where $\bar{\boldsymbol{D}}$ is a discrete approximation of the rate-of-strain tensor $\boldsymbol{D}$ obtained from Eq. 8. If the exact solution is recovered, this elliptic operator vanishes. However, in a finite element calculation this is generally not the case.

Problem 1 (DEVSS-G/SUPG)
Find $\boldsymbol{G}$, $\boldsymbol{\tau}$, $\boldsymbol{u}$, p such that for all admissible weighting functions $\boldsymbol{E}$, $\boldsymbol{S}$, $\boldsymbol{v}$, and q:

$$\left(\boldsymbol{S} + \alpha \boldsymbol{u} \cdot \nabla \boldsymbol{S},\ \lambda\left(\frac{\partial \tau}{\partial t} + u \cdot \nabla \tau - \boldsymbol{G} \cdot \tau - \tau \cdot \boldsymbol{G}^T\right) + \tau - \eta\left(\boldsymbol{G} + \boldsymbol{G}^T\right)\right) = 0 \tag{5}$$

$$\left(\left(\nabla \boldsymbol{v}\right)^T,\ \bar{\eta}\left(\boldsymbol{D} - \frac{1}{2}\left(\boldsymbol{G} + \boldsymbol{G}^T\right)\right) + \tau\right) - \left(\nabla \cdot v, p\right) = 0 \tag{6}$$

$$\left(q,\ \nabla \cdot \boldsymbol{u}\right) = 0 \tag{7}$$

$$\left(\boldsymbol{E},\ \left(\nabla \boldsymbol{u}\right)^T - \boldsymbol{G}\right) = 0 \tag{8}$$

If DEVSS-G/SUPG and a continuous interpolation of the extra stress tensor are used, the strain rate tensor (or the velocity gradient tensor) is interpolated in the same way as the extra stress tensor. The most commonly applied element for the DEVSS-G/SUPG method has a bi-quadratic velocity, bi-linear pressure, stress and strain rate (or velocity gradient) interpolation. This combination of interpolation spaces is also used in this work.

3 THE MAPPING METHOD

Several computational techniques can be used to track interfaces in fluid flows [25, 26]. These techniques can be separated into two broad categories: front capturing and front tracking. In the front capturing technique, massless markers are distributed within the fluid domain or a marker function is advected with the flow. The most difficult task within these approaches is to determine the location of the interface. Usually, it is recovered or "captured" using the calculated values of the marker function. The front tracking method on the other hand uses a separate moving mesh to describe the interface. Its location is accurately known at each time step. A disadvantage of both the front capturing and front tracking technique is that all computational work has to be repeated when the initial location of the interface changes. For passive interfaces, another method can be used to determine the evolution of the coextruded interface: the mapping method [27, 28].

The mapping method is based on front tracking, but the main difference is that this technique does not track each material volume over the total length z of the flow separately but

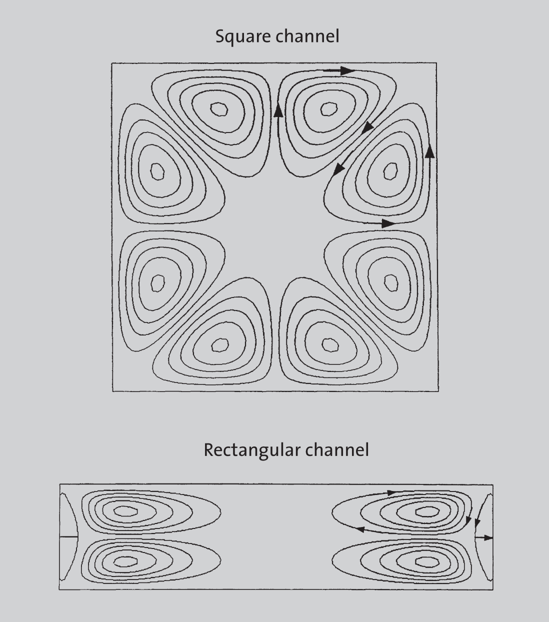

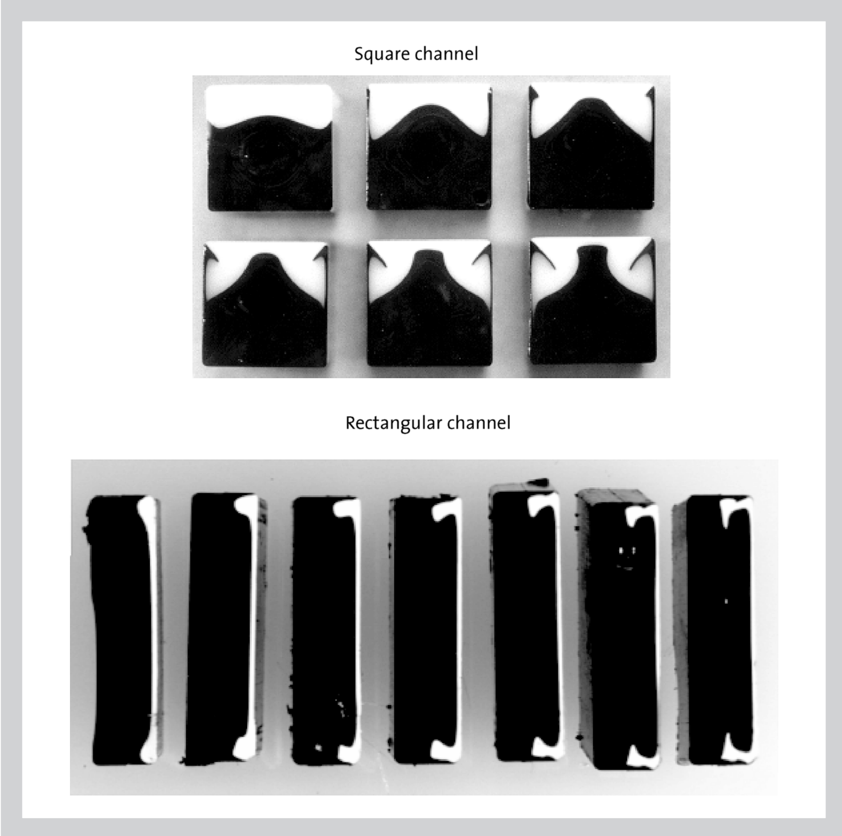

Figure 1 (left): Secondary flow in the axial cross section of the slit.

Figure 2: Experimental results showing the evolution of material in a square and rectangular channel.

instead creates a discretized mapping from a reference grid to a grid deformed during a relatively short representative length span Δz of the flow [29]. In the mapping method, the flow domain is divided into non-overlapping subdomains with boundaries. This subdivision is fully decoupled from any velocity field discretization. The boundaries of the subdomains are tracked, using front tracking, in a flow field over a distance from $z = z_o$ to $z = z_o + \Delta z$. Then the mapping from the initial grid to the deformed grid is constructed by determining the fraction of each cell of the deformed grid back in to the initial cells. The result is stored in a matrix Φ with size $n \times n$, where n is the number of cells in the grid. The accuracy of the method depends on the accuracy of the velocity field, and on the grid size n and mapping step Δz [27].

Once the matrix Φ is known, the advection of any initial color distribution, stored in a vector C_o of length n, is easily determined by the matrix vector multiplication providing the structure after Δz, yielding C_1. The advection after $2\Delta z$, C_2, is determined by multiplying Φ with C_1, and so on for $N\Delta z$ to arrive at the total flow length Δz. Using this technique, the interface location for coextruded structures with identical materials in each layer can easily be determined. In this work the mapping method is applied to determine the progression of the coextruded interface for the square and rectangular channel geometries.

4 RESULTS

4.1 FLOW

Figure 1 shows the predicted secondary flows in a square and in a rectangular channel for a viscoelastic fluid. For the fluid flowing through a square channel contain eight recirculation zones or vortices of roughly the same size are found, two each per quadrant. For the flow in the rectangular channel four larger and two smaller vortices appear. The flow patterns appear to correspond well with the interface deformation shown for the polystyrene resin in Fig. 2 where experimental results are shown for the flow in a square and rectangular channel [30, 31]. Here, two-layer coextruded structures were made using the same polymer in each layer with different colored pigments added to each layer to determine the location of the interface. A series of experiments were conducted that showed that the addition of the pigments at the loadings used in these experiments did not affect the flow properties of the resins and that the starting interface was indeed flat [32]. The interesting aspect of the layer rearrangement shown in Fig. 2 is that everywhere in the duct the same material flows and that thus viscous encapsulation is not the driving force. In case of viscous encapsulation the materials flow down the channel as the less viscous material encapsulates the more viscous material and an energetically preferred state is reached.

4.2 APPLICATION OF THE MAPPING METHOD

The polystyrene resin of Figs. 1 and 2 was simulated using the Giesekus constitutive Eq. 3. Based on the dynamic rheological properties of the polystyrene resin at a temperature of 204°C, a

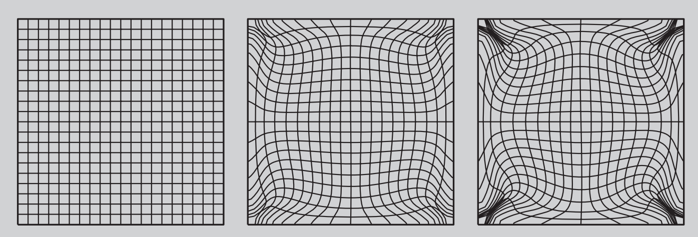

I	λ_i [s]	η_i [Poise]	α_i
1	10^2	23740	0.86
2	10^1	97670	0.48
3	10^0	163500	0.56
4	10^{-1}	44640	0.53
5	10^{-2}	8540	0.51

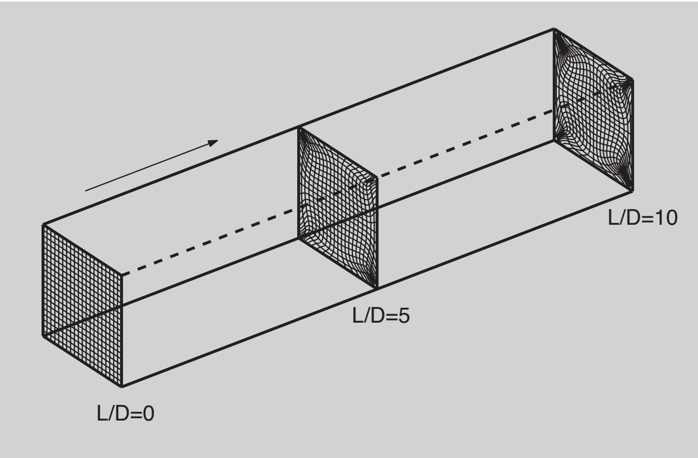

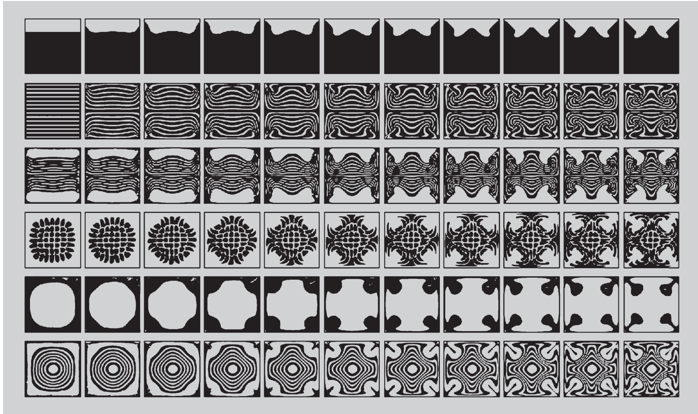

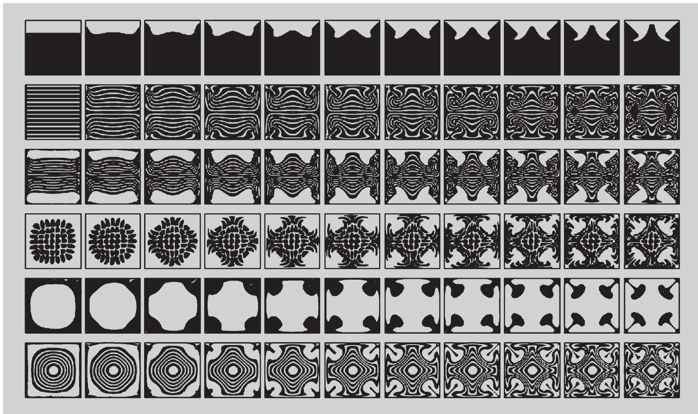

Table 1:
Material parameters for the Giesekus model with five relaxation times for polystyrene.

Figure 3 (left above):
The figure on the left shows a coarse initial mapping grid consisting of 20 × 20 cells. The figures in the middle and the right show the deformation of the grid in (a) after 5 L/D and 10 L/D respectively. The actual mapping grid contains 400 × 400 cells.

Figure 4 (left below):
Schematic figure showing the initial grid and the deformed grids after L/D = 5 and L/D = 10 in the channel.

Figure 5 (right above):
Interface deformation evolution of six different initial (column wise) structures in a square channel. Each subsequent figure in a row shows the progression after a multiple of 5 L/D. The last column contains the extruded structure after 50 L/D. The flow rate was 0.72 cc/s.

Figure 6 (right below):
Interface deformation evolution of six different initial (column wise) structures in a square channel. Each subsequent figure in a row shows the progression after a multiple of 5 L/D. The last column contains the extruded structure after 50 L/D. The flow rate was 2.48 cc/s.

discrete spectrum of five relaxation times λ_i ranging from 10^{-2} to 10^2 seconds was chosen. The corresponding partial viscosities η_i were fitted on the basis of the dynamic properties of the storage and loss moduli (*G'* and *G''*, respectively) while the α_i parameters were selected based on the viscosity [33]. Table 1 shows the values for the material properties used in the model. Two different volumetric flow rates were considered: a low flow rate of 0.72 cc/s and a high flow rate of 2.48 cc/s.

A finite element method was applied to determine the velocity field in the channels and the DEVSS/G-SUPG technique in combination with a theta-scheme was used to march in time to the steady state in the channel. Details of this method can be found in [34]. The finite element mesh consisted of 20 × 20 × 2 elements and the volumetric flow rate was prescribed via a Lagrange multiplier.

Based on the determined velocity field the mapping technique was applied and Figs. 3 and 4 illustrates they way the technique works by showing the deformation of a (in this example very coarse) grid consisting of 20 × 20 cells after 5 *L/D* and 10 *L/D*, where *D* is the width of the channel and *L* its length. The deformation of the grid follows the secondary flow field patterns shown in Fig. 1. Note that a comparison of a single cell in the three grids shows that the area of a cell is *not* preserved during deformation, however the flux through each cell is preserved. The actual computations are done on a much finer grid, i.e. 400 × 400 cells, and the mapping matrices created after 5 *L/D* and 10 *L/D* are combined to determine the evolution.

4.3 MAPPING RESULTS FOR THE SQUARE CHANNEL

Results of the mapping operation on different initial layer configurations in the square channel are

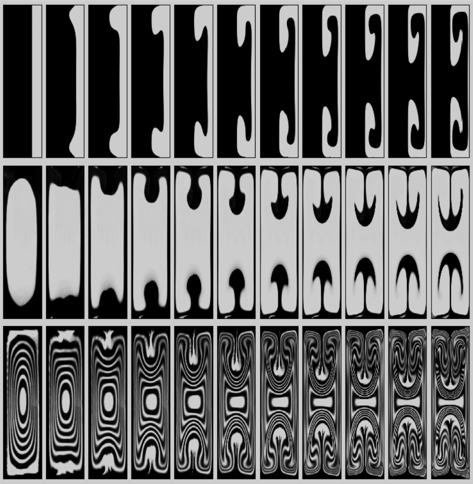

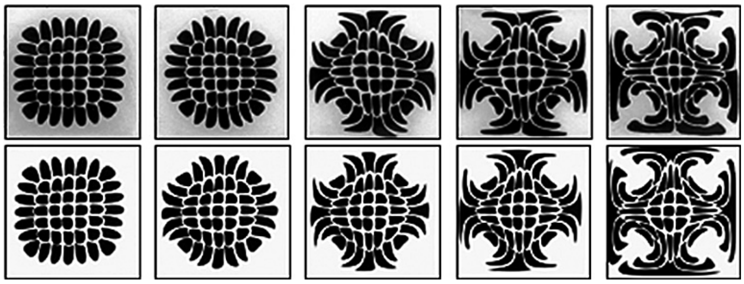

Figure 7 (left): Interface deformation evolution of three different initial (column wise) structures in the rectangular channel. Each subsequent figure shows the progression after a multiple of 5 L/D. The last column contains the extruded structure after 50 L/D. The flow rate was 2.48 cc/s.

Figure 8: Comparison of experimental (top row) and numerical results (bottom row) for the progression of a 49-strand polystyrene structure as it flows down a square channel. Excellent agreement is observed.

shown in Fig. 5 (low flow rate) and Fig. 6 (high flow rate), respectively. These initial layer configurations are based on experimental structures developed and evaluated previously [24]. These results show the effect of secondary flows on viscoelastic polymers as they flow through a square channel. All results are computed quickly (typically less than 1 CPU second on a standard PC) once the mapping matrix is determined. As was concluded from experimental results in previous work, the dependence of layer deformation on the flow rate is small [24]. Furthermore, it can be concluded that by applying the mapping method, the details of the deformation patterns are accurately resolved.

4.4 MAPPING RESULTS FOR THE RECTANGULAR CHANNEL

Figure 7 shows the results of the layer interface deformation in the rectangular channel. These results are similar to those in the square channel but the location and magnitude of the secondary flows have changed. As the aspect ratio of the channel gets larger, the recirculation zone associated with the longer side becomes larger while the recirculation associated with the smaller side is diminished. This shows how the secondary flows are affected by the aspect ratio of the channel. We have not investigated the influence of the aspect ratio of the channel in great detail. The topological structure of the secondary flow changes upon increase of the aspect ratio; the effect of the second-normal stresses can be reduced greatly. The effect of more practical die shapes, such as circular, teardrop, and leaking rectangular shaped channels was investigated experimentally already by Dooley [24].

4.5 COMPARISON OF EXPERIMENTAL AND COMPUTATIONAL RESULTS

Figure 8 shows experimental and numerical interface deformations for the progression of a 49-strand polystyrene structure as it flows down a square channel. The top row images are experimental samples showing the progression of a 49-stand polystyrene structure as it flows down the square channel. The bottom row are the numerical predictions at the same channel cross sections. The first column are images taken near the entry of the channel while the images in the last column are located near the exit of the channel.

This figure shows excellent agreement between the experimental and numerical results. This is the most complex structure of the three examined since an interface location must be determined for each of the 49 strands as they flow down the channel. However, even though this is the most complex structure, it appears that the mapping method was able to predict the strand deformation very accurately at each location down the channel.

4.6 INFLUENCE OF SECOND-NORMAL STRESS DIFFERENCE

In order to determine whether the present experimental technique could, ultimately, be used as a measure of the second-normal stress difference at high flow rates, a number of simulations were performed with different levels of viscoelasticity. The square channel geometry was chosen for these simulations since it produces strong secondary flow effects. For these simulations, the channel width and height were set to 1, the dimensionless flow rate was set to 1 as was the relaxation time. The level of viscoelasticity was changed by changing the non-linear α parameter in the single mode Giesekus model from 0.2 to 0.8 with steps of 0.2. The mapping matrices were computed for L/D = 10. Mapping was applied up to 20 times, yielding results up to L/D = 200. The initial (color) distribution was chosen such that the most reliable deformation patterns (from the corners to the center) were visualized.

The results of these simulations are shown in Fig. 9. The pointed parts of the lines on the diagonals are numerical artifacts that could be solved by grid refinement. It can be concluded from numerical experiments like these that the relative

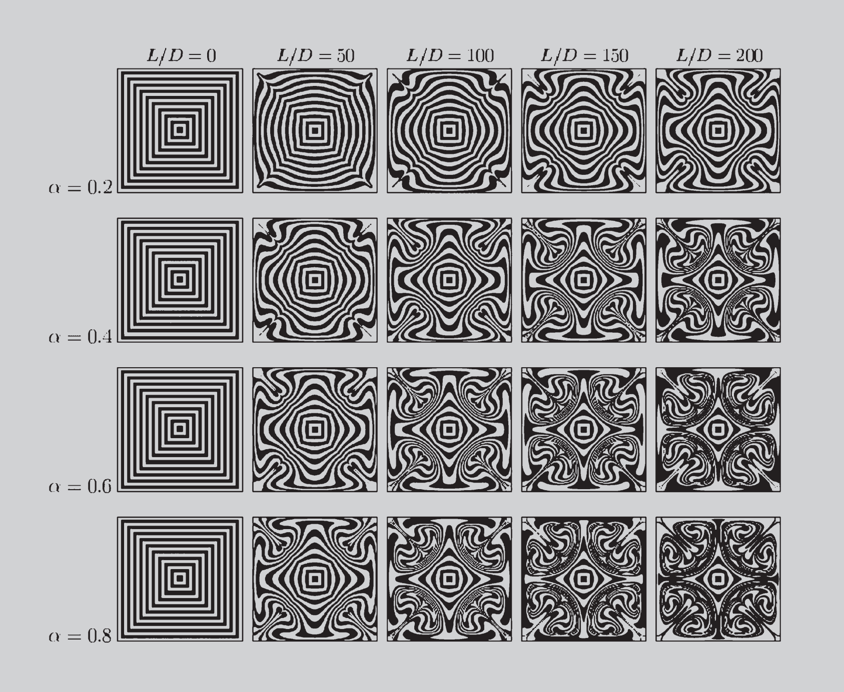

Figure 9: Numerical simulations comparing layer rearrangement as a function of distance traveled down a square channel. The viscoelasticity was changed by changing the non-linear α parameter in the one mode Giesekus model from 0 to 0.8 with steps of 0.2.

level of viscoelasticity can indeed be determined based on the amount of layer deformation caused by second-normal stress difference driven flows. These results indicate that the technique can be used to determine the second-normal stress difference under realistic flow rates by applying he technique in an inverse way. It is suggested by these results that (for this flow rate) a channel length of $50 < L/D < 100$ should be chosen to differentiate the level of viscoelasticity. Via an iterative numerical and experimental approach, these flows could even help to design improved constitutive equations that can quantitatively predict second normal stresses over a broad range of deformation rates. Note that the secondary flow-induced deformations are (sensitive) *integrals* of the velocity field over time, rather than (non-sensitive) *differentials*, which are stresses.

5 CONCLUSIONS

The mapping method was used to determine interface locations for coextruded polystyrene structures as they flow through square and rectangular channels. Excellent agreement between the experimental and numerical results was obtained. These results show the power of the mapping technique in determining interface deformation in monolithic coextruded structures. Moreover, the simulation results suggest that the technique can be used to determine the second-normal stress difference under realistic flow rates.

Clearly, the flow-induced patterning method which was demonstrated here would be more useful if part of the polymer is provided with additional functionality, such as electrical conductivity to be used for LED or capacitor applications. Other possibilities include a controlled difference in the refractive indices of the different structures to control optical properties.

REFERENCES

[1] Southern JH, Ballman RL: Stratified bicomponent flow of polymer melts in a tube. Appl. Polym. Sci. 20 (1973) 175.
[2] White JL, Ufford RC, Dharod KR, Price RL: Experimental and theoretical study of the extrusion of two-phase molten polymer systems. J. Appl. Polym. Sci. 16 (1972) 1313.
[3] Han CD: A study of bicomponent coextrusion of molten polymers. J. Appl. Polym. Sci. 17 (1973) 1289.
[4] Everage Jr AE: Theory of stratified bicomponent flow of polymer melts. 1. Equilibrium newtonian tube flow. Trans. Soc. Rheol. 17 (1973) 629.
[5] Karagiannis A, Hrymak A, Vlachopoulos J: Three-dimensional studies on bicomponent extrusion. Rheologica Acta 29 (1990) 71–87.
[6] Xue SC, Phan-Thien N, Tanner RI: Numerical study of secondary flows of viscoelastic fluid in straight pipes by an implicit finite volume method. J. Non-Newtonian Fluid Mechanics 59 (1995) 191–213.
[7] Takase M, Shinichi K, Funatsu K: Three-dimensional viscoelastic numerical analysis of the encapsulation phenomena in coextrusion. Rheologica Acta 37 (1998) 624–634.
[8] Sunwoo KB, Park SJ, Lee SJ, Ahn KH, Lee SJ: Numerical simulation of three-dimensional viscoelastic flow using the open boundary condition method in coextrusion process. J. Non-Newtonian Fluid Mechanics, 99 (2001) 125–144.
[9] Sunwoo KB, Park SJ, Lee SJ, Ahn KH, Lee SJ: Three-dimensional viscoelastic simulation of coextrusion process: Comparison with experimental data. Rheologica Acta 41 (2002) 144–153.
[10] Kim YJ, Han CD, Chin HN: Rheological investigation of interfacial instability in two-layer flat-film coextrusion. Polym. Eng. Rev. 4 (1984) 177.
[11] Arvedson MA: Rheological considerations in coextrusion. TAPPI/PLC Conference Proceedings 513 (1984) 84.
[12] Hickox CE: Instability due to viscosity stratification in axisymmetric pipe flow. Phys. Fluids 14(1971) 251.
[13] Yih CS: Instability due to viscosity stratification. J. Fluid Mech. 27 (1967) 337.
[14] Khan AA, Han CD: A study on the interfacial instability in the stratified flow of two viscoelastic fluids through a rectangular duct. Trans. Soc. Rheol. 21 (1977) 101.
[15] Hooper AP, Boyd WG: Shear-flow instability at the interface between two viscous fluids. J. Fluid Mech. 128(1983) 507.

[16] Schrenk WJ, Pinsky J: Coextruded iridescent film. TAPPI Paper Synthetics Proceedings (1976) 141–176.
[17] Han CD, Rao DA: Studies on wire coating extrusion. ii. the rheology of wire coating coextrusion. Polym. Eng. Sci. 20 (1980) 128.
[18] Alfrey T Jr., Schrenk WJ, Bradley NL, Maack H: Interfacial flow instability in multilayer coextrusion. Polym. Eng. Sci. 18 (1978) 620.
[19] Khomami B: Interfacial stability and deformation of two stratified Power law fluids in plane poiseuille flow. 1. stability analysis. J. Non-Newt. Fluid Mech. 36 (1990) 289.
[20] Khomami B: Interfacial stability and deformation of two stratified Power law fluids in plane poiseuille flow. 2. interface deformation. J. Non-Newt. Fluid Mech. 37 (1990) 19.
[21] Waters ND: The stability of two stratified Power-law liquids in couette flow. J. Non-Newt. Fluid Mech., 12 (1989) 85.
[22] Wilson GM, Khomami B: An experimental investigation of interfacial instabilities in multilayer flow of viscoelastic fluids. 1. Incompatible polymer systems. J. Non-Newt. Fluid Mech. 45 (1992) 355.
[23] Wilson GM, Khomami B: An experimental investigation of interfacial instabilities in multilayer flow of viscoelastic fluids. 2. Elastic and nonlinear effects in incompatible polymer systems. J. Rheol. 37 (1993) 315.
[24] Dooley J: Viscoelastic Flow Effects in Multilayer Polymer Coextrusion. Ph.D. thesis (2002) Eindhoven University of Technology.
[25] Hirt CV, Nichols BD: Volume of fluid (VOF) methods for the dynamics of free boundaries. J. Comput. Phys 39 (1981) 201–225.
[26] Unverdi SO, Tryggvason G: Computations of multi-fluid flows. Phys. Fluids D 60 (1992) 70–83.
[27] Kruijt PGM, Galaktionov OS, Anderson PD, Peters GWM, Meijer HEH: Analyzing fluid mixing in periodic flows by distribution matrices. AIChE J. 47 (2001) 1005–1015.
[28] Galaktionov OS, Anderson PD, Peters GWM, Tucker III CL: A global, multi-scale simulation of laminar fluid mixing: The extended mapping method. Int. J. Multiphase Flows 28 (2002) 497–523.
[29] Anderson PD, Meijer HEH: Chaotic mixing analyses by distribution matrices. Appl. Rheol. 10 (2000) 119–133.
[30] Dietsche L, Dooley J: Numerical simulation of viscoelastic polymer flow - effect of secondary flows on multilayer coextrusion. SPE-ANTEC Technical Papers 41 (1995) 188.
[31] Dooley J, Debbaut B, Avalosse T, Hughes K: On the development of secondary motions in straight channels induced by the second normal stress difference: Experiments and simulations. J. Non-Newtonian Fluid Mech. 69 (1997) 255.
[32] Hyun KS, Dooley J, Hughes KR: An experimental study on the effect of polymer viscoelasticity on layer rearrangement in coextruded structures. Polymer Engineering and Science 38 (1998) 1060.
[33] Martinez-Ruvalcaba A, Chornet E, Rodrigue D: Dynamic rheological properties of concentrated chitosan solutions. Appl. Rheol. 14 (2004) 140–147.
[34] Bogaerds ACB: Stability analysis of viscoelastic flows. Ph.D. thesis (2002) Eindhoven University of Technology.